ORIGINAL ARTICLE

Concurrent activation and surface modification (CAM) process to produce surface-modified palm kernel shell-derived activated carbon (PKSdAC)

Jia Yen Lai[1] · Jiuan Jing Chew[1] · Lock Hei Ngu[1]

Abstract

Activated carbon production via chemical activation followed by surface functionalization with metal groups aims to achieve surface functionalization for CO_2, aromatic/metallic organic compounds, and dye adsorption. The prepared activated carbon possesses a porous structure containing metal functional groups with adsorptive properties. This work proposed integrating two synthesis steps to simplify the process and reduce resources and impact. The preparation of palm kernel shell (PKS) derived AC (PKSdAC) through a concurrent activation and surface modification (CAM) process combines sulphuric acid (H_2SO_4) activation (5–10% mass loading) with barium chloride ($BaCl_2$) modification (10 wt.%) at an activation temperature of 400–700 °C. The barium (Ba) is produced through the reduction process. Incorporating Ba into PKSdAC is vital to initiate chemical CO_2 and other related component adsorption. The optimization study identified that 7.5% H_2SO_4, 10 wt.% $BaCl_2$, and 700 °C was optimal in obtaining a high 1.50 wt.% Ba impregnated in PKSdAC. CAM-PKSdAC synthesized at optimal conditions exhibited a sponge-like cubic meso-microporous carbon structure containing $BaSO_4$ crystals with a surface area of 420 and 423 m^2 g^{-1} for its micropore and mesopore structure. A total pore volume of 0.19 cm^3 g^{-1} and an average pore diameter of 1.78 nm were achieved. Conventional surface modified-activated PKSdAC prepared at optimal conditions has a cubic porous structure and a crack surface containing little $BaSO_4$ crystals with a higher surface area of 565 m^2 g^{-1} and total pore volume of 0.18 cm^3 g^{-1} and an average pore diameter of 1.27 nm.

Keywords Integrated synthesis process · Chemical activation · Ba surface groups · Central composite design · Voids formation

1 Introduction

Oil palm biomass-derived activated carbon is a potential adsorbent for applications in removing organic pollutants from water, treatment of heavy metal from wastewater, liquid adsorption, reduction of gaseous pollutants emission, and, more recently, carbon dioxide (CO_2) adsorption [1–7].

Palm kernel shell (PKS) is an attractive precursor for the synthesis of AC, given its high carbon, high lignin, significant volatile materials, and low ash content in addition to its hard and rough surfaces [8, 9]. Generally, PKS-derived

AC (PKSdAC) can be prepared by three activation processes: physical, chemical, and physiochemical activation. The physical activation of PKS is performed after the carbonization process under the presence of oxidizing gas at an elevated temperature of 800–1100 °C [10–12]. The chemical activation process initially soaks PKS in a chemical dehydrating agent, followed by simultaneous carbonization and activation at a temperature range of 400–800 °C [9, 11–13]. Physiochemical activation is a process combining physical and chemical activation. The PKS undergoes chemical impregnation before the gasification with oxidizing gas [9, 11–13]. Chemical activation is cost-friendly among the activation processes from cost evaluation by Lai et al. [14]. The chemical activation does not use expensive and high-risk oxidizing gas. PKSdAC with higher surface area and smaller micropores have been prepared by chemical activation [15]. In addition, other than a chemical dehydrating

✉ Lock Hei Ngu
lngu@swinburne.edu.my

[1] Research Centre for Sustainable Technologies, Faculty of Engineering, Computing and Science, Swinburne University of Technology, Jalan Simpang Tiga, 93350 Kuching, Sarawak, Malaysia

agent, washing of PKSdAC can be carried out using distilled water to reduce the overall operational cost [16, 17].

Tian et al. [18] synthesized waste cotton-derived AC via chemical activation with a mixture of $FeCl_3$ and $ZnCl_2$. The dehydration of $ZnCl_2$ and $FeCl_3$ is responsible for pores development on the cotton waste precursor. The AC achieved a high surface area of 1342 m^2 g^{-1}, micropore volume of 0.45 cm^3 g^{-1}, and mesopore size of 2.00 nm. Sun et al. [19] used ferric chloride hexahydrate ($FeCl_3 \cdot 6H_2O$), aluminium chloride hexahydrate ($AlCl_3 \cdot 6H_2O$), and manganese chloride tetrahydrate ($MnCl_2 \cdot 4H_2O$) as activating agent incorporated with H_3PO_4 activation to prepare Arundo donax Linn-derived AC. The AC prepared by $MnCl_2$-H_3PO_4 activation yielded the highest BET surface area (1332 m^2 g^{-1}) and the highest total pore volume (1.06 cm^3 g^{-1}) with a mesopore size of 3.18 nm compared to those prepared by H_3PO_4 mixed with $FeCl_3$ activation (BET surface area = 1156 m^2 g^{-1}, total pore volume = 1.03 cm^3 g^{-1}, and pore size = 3.55 nm) and H_3PO_4 mixed with $AlCl_3$ activation (BET surface area = 992 m^2 g^{-1}, total pore volume = 0.69 cm^3 g^{-1}, and pore size = 2.77 nm). Amuda and Ibrahim [20] studied the removal of chemical oxygen demand (COD) on $BaCl_2$-activated coconut shell carbon, and Ajani et al. [21] investigated the adsorption of methylene blue from aqueous solution onto the mango seed shells-based AC prepared using $BaCl_2$ activation. Both $BaCl_2$-activated coconut shell ACs and $BaCl_2$-activated mango seed shell ACs are suitable as adsorbents for COD and methylene blue adsorption via physisorption with good adsorption efficiency towards dye and organic matter.
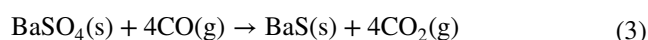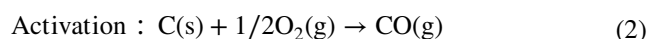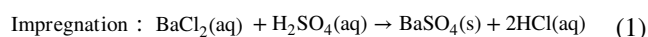
Surface modifications are typically implemented after the activation process to alter the surface chemistry of PKSdAC. Nitrogen incorporation or metal functionalization of PKSdAC are amongst the surface modification adopted to enhance adsorption performance [15]. Amine modification incorporates nitrogen groups into PKSdAC using mild-temperature drying [22, 23]. The surface functionalization of metal nanoparticles on PKSdAC is performed using a high-temperature thermal process [24, 25]. The impregnated metal nanoparticles retained in porous PKSdAC and on the surface enhance the chemical adsorption performance and selectivity of CO_2 via electrostatic interactions [26]. The existing post-synthetic surface modification methods on PKSdAC are disadvantageous by requiring a subsequent additional step and complex synthesis process for a prolonged time. The post-synthetic surface modification causes reduced surface area and pores in the prepared PKSdAC. To our knowledge, there are limited studies of single-step chemical activation and surface modification with a mix of activating agents [18, 19].

In this work, concurrent activation and surface modification (CAM) using barium salt ($BaCl_2$) as the modifying agent with H_2SO_4 activating agent for the preparation of surface-modified AC from palm kernel shell (PKS) is presented. The concurrent activation and modification (CAM) process involves simultaneous activation and surface modification. Compared to conventional surface modified-activated PKSdAC production, the CAM process reduces the overall production cost by 12% by eliminating the subsequent additional thermal surface modification based on a 10,000 kg day^{-1} feed [27]. Incorporating basic functional groups, such as barium (Ba), on the PKSdAC will improve surface adsorption properties [28], including the chemical adsorption of CO_2 [18–21]. The presence of basic metal surface groups on PKSdAC serves as an electron donor via donating the lone pair of electrons to increase the chemisorption of acidic CO_2 [29]. The deposition of barium (Ba) on the surface and pores of the derived AC was achieved via the reduction of barium sulphate ($BaSO_4$) (i.e., from H_2SO_4 and $BaCl_2$) to barium sulphide (BaS) [30].

Figures 1(a) and (b) illustrates the CAM and the conventional process of carbonaceous material to obtain targeted surface functional groups (i.e., acidic and metal surface functional groups). Mechanism (I) presents the reaction mechanism of CAM process of carbonaceous material. $BaSO_4$ then reacts with carbon in PKS with the net generation of carbon monoxide (CO) and carbon dioxide (CO_2) following the reaction scheme shown in Eqs. 2–4 [31, 32]. The chemical impregnation of H_2SO_4-treated PKS with $BaCl_2$ solution leads to the formation of $BaSO_4$ in the PKS (Eq. 1). The carbon (C) material combines with oxygen (O_2) in the air and partially oxidizes carbon to CO during the CAM process, as depicted by Eq. 2 [31, 32]. Subsequently, the $BaSO_4$ reduces to barium sulphide (BaS), oxidizing CO to CO_2 (Eq. 3) [30]. The Boudouard reaction is postulated to be the rate-controlling step of the overall reaction mechanism, as shown in Eq. 4 [32]. Equation 5 shows the general reduction reaction of $BaSO_4$ to BaS with carbon as the reducing agent [30]. This reduction process is important in forming BaS, an intermediate in producing barium (Ba) compounds [30, 33]. Although the reduction of $BaSO_4$ typically occurs at 600 °C [34], a small amount of carbon additives produced from the slow pyrolysis of PKS acts as the reducing agent. It enables the reduction to initiate below 400 °C [35].

(I) Mechanism of CAM process of carbonaceous material

$$\text{Impregnation}: BaCl_2(aq) + H_2SO_4(aq) \rightarrow BaSO_4(s) + 2HCl(aq) \tag{1}$$

$$\text{Activation}: C(s) + 1/2O_2(g) \rightarrow CO(g) \tag{2}$$

$$BaSO_4(s) + 4CO(g) \rightarrow BaS(s) + 4CO_2(g) \tag{3}$$

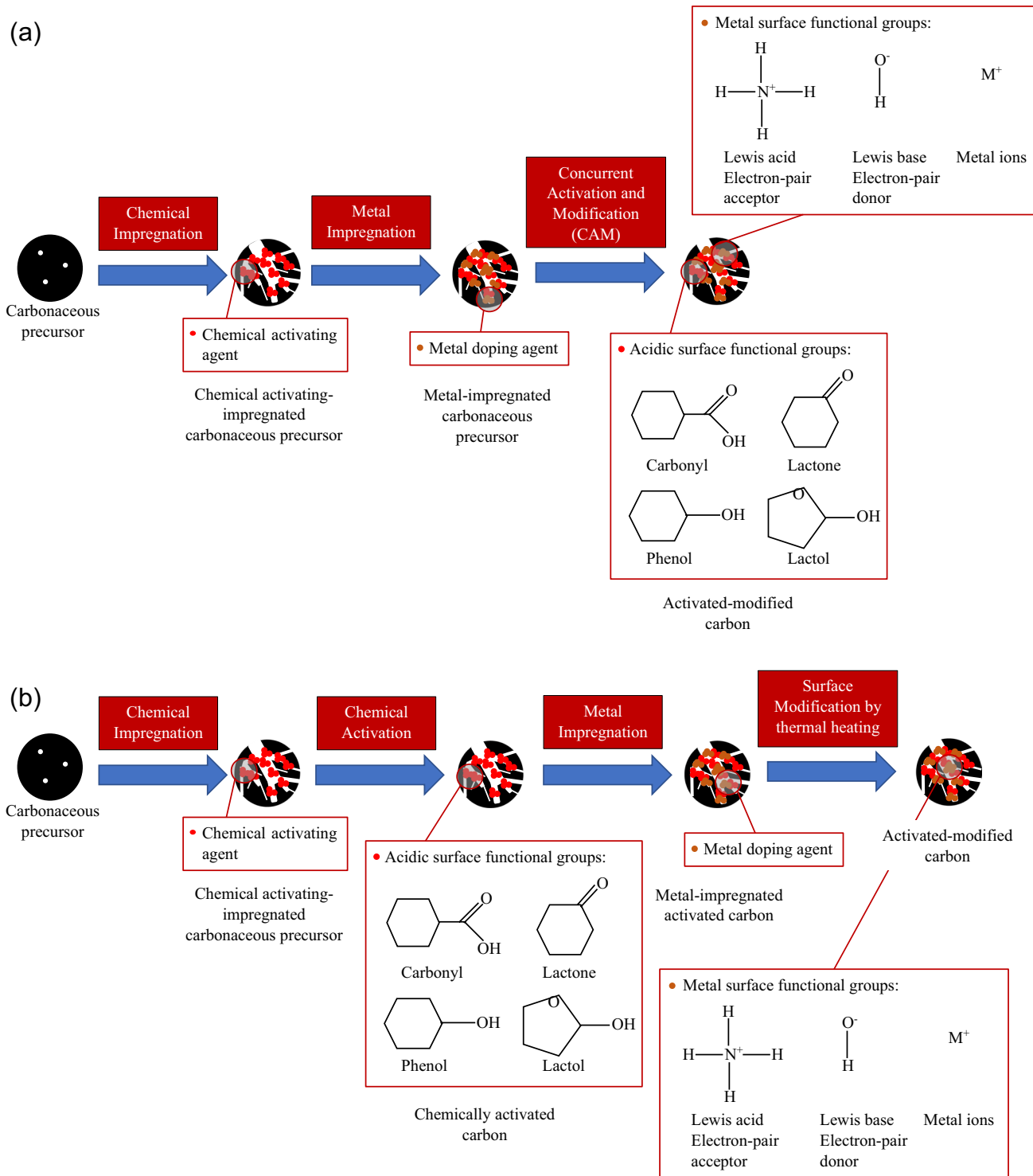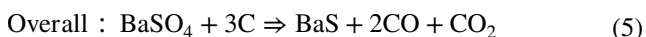$$C(s) + CO_2(g) \leftrightarrow 2CO(g) \tag{4}$$

Fig. 1 Illustration of (**a**) concurrent activation and surface modification (CAM) process and (**b**) conventional chemical activation-surface modification process
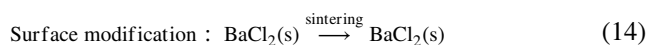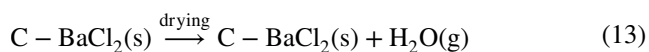
$$\text{Overall}: BaSO_4 + 3C \Rightarrow BaS + 2CO + CO_2 \quad (5)$$

The reaction mechanism of the conventional process of carbonaceous material is shown in mechanism (II). The

impregnation of H_2SO_4 incorporates H_2SO_4 compound into the interior of PKS (Eq. 6). After drying, moisture is removed from the PKS, and H_2SO_4 remains as liquid in the PKS structure (Eq. 7). During H_2SO_4 activation,

water vapor formed from H_2SO_4 dehydration burns off the carbon content of PKS through the gasification process to create substantial pore volumes an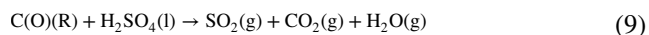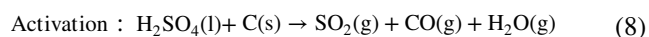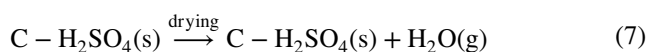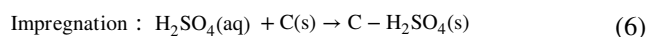d internal porosities [16]. Simultaneously, H_2SO_4 reacts with the $C = C$ bond in the derived carbon material to release gaseous SO_2, CO_2, and CO [36, 37] (Eq. 8). Equation 9 is the thermal decomposition reaction of oxygen-containing functional groups (C(O)), which are carboxyl, phenolic hydroxyl, and ester groups [37]. In the presence of O_2, carbon reacts with O_2 to produce CO (Eq. 10), while C(O) reacts with O_2 to release CO_2 (Eq. 11) [37]. The impregnation of chemically activated carbon with $BaCl_2$, followed by a subsequent drying process, causes $BaCl_2$ solid to penetrate the interior pores and beneath the AC surface (Eqs. 12–13). At a high-temperature thermal surface modification process, the sintering of $BaCl_2$ to $BaCl_2$ salts occupies the interior pores and the surface of AC (Eq. 14).

(II) Mechanism of conventional process of carbonaceous material

$$\text{Impregnation}: H_2SO_4(aq) + C(s) \rightarrow C - H_2SO_4(s) \tag{6}$$

$$C - H_2SO_4(s) \xrightarrow{\text{drying}} C - H_2SO_4(s) + H_2O(g) \tag{7}$$

$$\text{Activation}: H_2SO_4(l) + C(s) \rightarrow SO_2(g) + CO(g) + H_2O(g) \tag{8}$$

$$C(O)(R) + H_2SO_4(l) \rightarrow SO_2(g) + CO_2(g) + H_2O(g) \tag{9}$$

$$C(s) + O(g) \rightarrow CO(g) \tag{10}$$

$$C(O)(R) + O(g) \rightarrow CO_2(g) \tag{11}$$

$$\text{Impregnation}: BaCl_2(aq) + C(s) \rightarrow C - BaCl_2(s) \tag{12}$$

$$C - BaCl_2(s) \xrightarrow{\text{drying}} C - BaCl_2(s) + H_2O(g) \tag{13}$$

$$\text{Surface modification}: BaCl_2(s) \xrightarrow{\text{sintering}} BaCl_2(s) \tag{14}$$
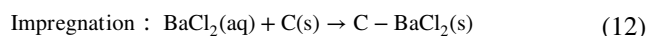
A response surface methodology (RSM) based on central composite design (CCD) was applied to optimize the mass ratio of PKS to H_2SO_4 (also termed H_2SO_4 mass loading) and the activation temperature for preparing AC in this work. In addition, the effect of $BaCl_2$ mass loading on the PKSdAC was also evaluated to determine the mass ratio of H_2SO_4-treated PKS to $BaCl_2$ to achieve a high amount of Ba impregnated on the PKSdAC. The PKSdAC was prepared at the optimal CAM conditions using a conventional H_2SO_4 activation followed by the subsequent $BaCl_2$ surface modification process. It acts as a control sample to compare the

impregnated Ba amount and its textural characteristics to the optimum CAM-PKSdAC.

2 Experimental section

2.1 Materials

Palm kernel shell (PKS) biomass was obtained from Lambir Palm Oil Mill in Miri Sarawak, Malaysia. The PKSs were pulverized to a particle size of 2 mm using a rotor mill (FRITSCH, Malaysia) and manually sieved using a test sieve (FRITSCH, Subang Jaya, Malaysia) with a diameter of 500 μm. The PKS was washed and dried in an oven (BINDER GmbH, Tuttlingen, Germany) at 105 °C for 24 h. The dried PKS was stored at room temperature in sealed containers before the experiments. Sulphuric acid (H_2SO_4, 95–98% purity, R&M) was used as an activating agent, while barium chloride ($BaCl_2$, ≥ 99% purity, Merck) was used as the modifying agent in the CAM process.

2.2 Concurrent activation and modification (CAM)

The synthesis of PKSdAC via the two-stage integrated CAM process was conducted according to our parametric study [38]. In the parametric study, CAM was performed at activation temperatures of 400 °C, 550 °C, and 700 °C using 10% and 30% H_2SO_4 mass loading. The findings from the parametric study showed that CAM-PKSdAC prepared using 10% H_2SO_4 mass loading successfully synthesized and impregnated the highest Ba amount (2.98 wt.%), compared to using 30% H_2SO_4 mass loading (0.86 wt.%). A lower H_2SO_4 mass loading postulates to incorporate a higher Ba amount on CAM-PKSdAC. A further investigation of the effect of lower H_2SO_4 mass loading (i.e., 5–10%) on Ba functionalization of CAM-PKSdAC was therefore carried out.

48 g raw PKS was pulverized and sieved into 2 mm particles. The PKS was washed to remove residual sand and fibers and then dried in an oven (BINDER GmbH, Tuttlingen, Germany) at 105 °C for 24 h. After drying, the PKS was soaked in a 5% H_2SO_4 solution (R&M, United Kingdom) at ambient temperature for 48 h for homogeneous chemical impregnation. The PKS was separated from the H_2SO_4 solution by vacuum filtration, followed by drying at 110 °C for 8 h to remove residual H_2SO_4. Subsequently, the PKS underwent metal impregnation following the published work on the surface modification of PKSdAC using metal impregnation [24]. A 10 wt.% $BaCl_2$ solution (Merck, United States) was used to impregnate PKS at ambient temperature for about 24 h. After metal impregnation, the PKS was dried at 70 °C for 24 h using the oven. It was simultaneously activated and thermally modified in a muffle furnace (Carbolite, Derbyshire, United Kingdom) at 400 °C for 2 h to produce PKSdAC. After

cooling down, the PKSdAC was collected and washed several times to reduce $BaCl_2$ content until the solution reached a stable pH value within 7–8. The wet PKSdAC was dried at 110 °C for 24 h and stored for material characterization.

The CAM process was repeated to synthesize PKSdAC by adjusting the H_2SO_4 mass loading to 7.5% and 10% and activation temperature to 550 °C and 700 °C, as specified by the designed experimental runs in Table S1. The experimental runs were repeated twice. The CAM-PKSdAC samples were labelled as CxH$_2$SO$_4$-PKSdAC-T, where x is the H_2SO_4 mass loading (i.e., 5%, 7.5%, and 10%), and T is the activation temperature (i.e., 400, 550, and 700 °C).

The preparation of conventional surface modified-activated PKSdAC was prepared via 2-step H_2SO_4 activation followed by subsequent $BaCl_2$ surface modification as following the synthesis procedure in our techno-economic feasibility study [27]. The PKS was first impregnated in a 7.5% H_2SO_4 solution at ambient temperature for 48 h and dried at 110 °C for 8 h before it was activated at 700 °C at a heating rate of 10 °C min^{-1} in a muffle furnace (Carbolite, Derbyshire, United Kingdom) for 2 h to produce PKSdAC. After activation, the PKSdAC was soaked in a 10 wt.% $BaCl_2$ solution at ambient temperature for about 24 h. The $BaCl_2$-impregnated PKSdAC was dried at 70 °C for 24 h and then heated at 750 °C for 1 h for surface modification. The resultant surface-modified PKSdAC underwent washing until the solution reached a stable pH within 7–8. Lastly, the surface-modified PKSdAC was dried at 110 °C for 24 h before storage for material characterization.

The conventional surface modified-activated PKSdAC was prepared as the control sample to compare the Ba impregnation outcome (i.e., CAM against conventional chemical activation-surface modification process). The conventional surface modified-activated PKSdAC was labelled as CxH$_2$SO$_4$-PKSdAC-T-modified, where x is 7.5% H_2SO_4 mass loading, and T is the activation temperature of 700 °C.

2.3 Correlation and optimization study of CAM-PKSdAC synthesis

The CAM optimization study was performed with response surface methodology (RSM) based on face centered central composite design (CCD) using the testing range from the parametric study in previous work [38]. RSM is a numerical and statistical model tool utilized to assess the effect of the independent variables, individually or in combination

with the dependent variable (response). It requires minimum experimental runs to optimize the best experimental conditions for the CAM process of PKS [39]. Figure S1 illustrates the optimization study flow adopted in this study. CCD was employed to study the correlation and the individual and interactive effects of the CAM process parameters (i.e., activation temperature and H_2SO_4 mass loading) toward the production of PKSdAC and its potential barium (Ba) loading. CCD enables the response surface within vicinity of the center points to be effectively explored while providing information about the interaction effects between factors. This make CCD design a promising tool for the optimization of activation temperature and H_2SO_4 mass loading with a fractional factorial design to produce PKSdAC impregnated with a high Ba amount [40]. Table 1 illustrates the process parameters and factor levels for the two CAM experiments. In Table 1, H_2SO_4 mass loading (5–10%) (B) and activation temperature (400–700 °C) (A) varied over three levels. The factor levels were denoted as -1 (low), 0 (central point), and + 1 (high). The impregnated Ba amount was analyzed as the response. Table S1 summarizes the nine experimental runs obtained from CCD based on the two CAM process parameters and their factor levels. A total of nine experiments were carried out to investigate the influence of the CAM process parameters on impregnated Ba amount. The impregnated Ba amount from experiments was used for the correlation study analysis. The results were analyzed with 95% confidence intervals using the Analysis of Variance (ANOVA) from Design Expert 6.0.10 software. After the correlation study, CAM process conditions were optimized using a numerical method. The interpretation of correlation and optimization study analysis are presented in Section 3.2.

2.4 Effect of barium mass loading on CAM-PKSdAC

The optimal synthesis condition identified from the RSM in Section 2.3 is adopted to study the mass loading effect (2, 4, 6, 8, and 10 wt.%) of surface modification agents ($BaCl_2$) on the impregnated Ba on PKSdAC. The $BaCl_2$ mass loading was studied to investigate whether lower $BaCl_2$ mass loading was adequate to achieve a comparable impregnated Ba amount using 10 wt.% of $BaCl_2$. The CAM-PKSdAC samples were labelled CxH$_2$SO$_4$-PKSdAC-T-yBaCl$_2$, where y is the $BaCl_2$ mass loading.

Table 1 Experimental design with 2 factors and 3 levels

Variables	Symbol	Coded factor levels		
		Low value (-1)	Central point (0)	High value (+ 1)
Activation temperature (°C)	A	400	550	700
H_2SO_4 mass loading (%)	B	5.00	7.50	10.00

2.5 Characterization of CAM-PKSdAC

For the nine CAM-PKSdAC produced with different H_2SO_4 loading (i.e., 5%, 7.5%, and 10%) and the optimum CAM-PKSdAC, the amount of the impregnated Ba in the CAM-PKSdACs was analyzed through inductively coupled plasma-optical emission spectrometry (ICP-OES) using USEPA 6010 B method [41]. Before the analysis, the CAM-PKSdAC was digested through conventional wet acid digestion per USEPA 3050 B method [42]. The sample digestion was to digest standard reference materials and the surface of the CAM-PKSdAC to ensure Ba does not degrade during extraction.

The pore structures of the optimum CAM-PKSdAC were characterized using N_2 physisorption at 77 K to obtain adsorption isotherms by performing the test using Micromeritics ASAP 2020 apparatus (Micromeritics Instrument Corporation, Norcross, United States) [43]. The surface area was calculated by the BET method (S_{BET}), while the total pore volume (V_{total}) was determined from the nitrogen amount adsorbed at a relative pressure (P/P_0) of 0.99 [44, 45]. The average pore diameter (D_{avg}) of the optimum CAM-PKSdAC was calculated using the measured S_{BET} and V_{total}. Micropore volume (V_{micro}) was obtained from the t-plot analysis [44, 45]. The mesopore volume and size distribution were determined by the Barrett-Joyner-Halenda (BJH) method from the N_2 adsorption data [44, 45].

A variable-pressure scanning electron microscope (VP-SEM) using a scanning electron microscope model JEOL JSM-IT300LV (JEOL USA Inc., Pittsfield, United States) at an accelerating voltage of 10 kV across the magnification range of 500X-2500X was used to characterize the surface morphology of the optimum CAM-PKSdAC [46].

Elemental contents such as carbon (C), hydrogen (H), nitrogen (N), and sulphur (S) of raw PKS and the optimum CAM-PKSdAC were analyzed using a CHNS analyzer model FlashSmart CHNS/O (Thermo Fisher Scientific, Shah Alam, Malaysia). The crystallinity of the optimum CAM-PKSdAC was characterized by X-ray diffraction (XRD) method [46]. The model D8 Advance X-Ray Diffractometer-Bruker (Bruker Corporation, Billerica, United States) was operated at 40 kV, 15 mA at ambient temperature to calculate its diffractogram and lattice constant/indexing using DIFFRAC plus-EVA software.

The organic functional groups in the optimum CAM-PKSdAC were characterized by ex-situ Fourier Transform Infrared (FTIR) Spectroscopy using spectrometer model IFS66v/S (Bruker Optics, Ettlingen, Germany) with software Bruker Optic GmBH 19972000 OPUS Version 3.1. This was performed via the attenuated total reflectance (ATR) method to determine the presence and absence of structural and compositional in the CAM-PKSdAC [47]. The spectra were recorded within a wave number of 400–4000 cm^{-1}.

The conventional surface modified-activated PKSdAC was also characterized for the impregnated Ba amount by ICP-OES, the BET surface area and pore structure, its morphology and crystallinity using VP-SEM and XRD, the C, H, N and S elemental contents, and the presence of organic functional groups on its surface via FTIR.

3 Result and Discussion

3.1 Correlation and optimization study of the synthesis of CAM-PKSdAC

Figure 2 shows the effect of H_2SO_4 mass loading (5.0, 7.5, and 10%) and activation temperature (400, 550, and 700 °C) using 10 wt.% $BaCl_2$ on the amount of Ba impregnated in CAM-PKSdAC and a control sample, conventional surface modified-activated PKSdAC (C7.5H_2SO_4-PKSdAC-700-modified). Repeated measurements on the amount of Ba impregnated in the 9 samples of CAM-PKSdAC showed a standard deviation of 0.14–0.21 for 5% H_2SO_4 mass loading, 0.014–0.45 for 7.5% H_2SO_4 mass loading, and 0.053–0.34 for 10% H_2SO_4 mass loading for all activation temperature. The correlation study based on the designed experimental runs observed that CAM-PKSdAC treated with 7.5% H_2SO_4 and activation temperature of 700 °C exhibited the highest impregnated Ba amount of 1.50 wt.%. The conventional surface modified-activated PKSdAC has a lower impregnated Ba amount with 0.072 wt.% with a standard deviation of 0.012, compared to the CAM-PKSdACs, manifesting the integration of a two-step CAM process was possible to achieve Ba surface modification on PKSdAC. The CAM-PKSdAC showed a larger mass yield of 6.20 g than the conventional surface modified-activated PKSdAC, with a 5.40 g mass yield.

From Fig. 2, the impregnated Ba amount decreased with the increase in the H_2SO_4 mass loading when CAM-PKSdAC was treated at 400 °C and 550 °C, respectively. Whereas for CAM-PKSdAC treated at 700 °C, the impregnated Ba amount increased when the H_2SO_4 mass loading increased from 5.0% to 7.5%, and then the Ba amount reduced with increasing H_2SO_4 mass loading from 7.5% to 10%. When considering the effect of activation temperature, for 5.0%, 7.5%, and 10% H_2SO_4 mass loading, the impregnated Ba amount decreased as the activation temperature increased from 400 °C to 550 °C, then increased with a further increase to 700 °C. Activation temperature affects the amount of carbon derived from PKS, since several reactions can occur over the range of 400 °C to 700 °C, alongside $BaSO_4$ reduction (i.e., $BaSO_4$ reduction was initiated at the temperature range 400–700 °C) [30, 33, 35]. This consequently affects the amount of Ba impregnated on PKSdAC.

The loss of moisture and the breakdown of complex organic compounds into smaller molecules, such as volatile gases, tar, and char, occurs mainly at temperatures below 500 °C [9]. The moderate amount of carbon with moisture and minor ash constituents (i.e., devolatilisation) in the char derived at 400 °C causes the $BaSO_4$ reduction to BaS [30]. As the temperature increases beyond this range, secondary reactions become more significant. With competing reactions (i.e., formation of secondary char and the $BaSO_4$ reduction using char as reducing agent), the impregnated Ba amount is reduced when PKS is activated at 550 °C for all H_2SO_4 mass loading [30, 35, 48, 49]. As the temperature increases further, greater volatile compounds are released, forming more carbon-rich species [9]. Consequently, at similar H_2SO_4 mass loading of 5.0%, 7.5%, and 10%, a high impregnated Ba amount was exhibited at 700 °C, followed by CAM-PKSdAC prepared at 400 °C then 550 °C. This indicates that an increased activation temperature of 700 °C was favourable for $BaCl_2$ surface modification on CAM-PKSdAC. However, the impregnated Ba amount at 700 °C showed a bell-shaped trend. The H_2SO_4 mass loading has a noticeable impact on the amount of Ba impregnated on CAM-PKSdAC. High H_2SO_4 mass loading (10%) was attributed to the scale formation of $BaSO_4$ precipitate that becomes saturated with PKS because $BaSO_4$ is highly insoluble [50]. At 700 °C, the presence of bulk $BaSO_4$ causes a change in the initiation temperature of the reduction process to form large BaS particles. The incompletion reduction process attributed to the remaining unreacted $BaSO_4$ on the CAM-PKSdAC, resulting in low Ba impregnation [30, 51].

The $BaSO_4$ reduction process occurs in the presence of air, causing a rapid increase in the re-oxidation rate of BaS with increasing temperature [53]. In addition, the Ba compound yield was unchanged or slightly increased by 1–2 wt.% when the reaction time was increased from 2 to 4 h for the reduction of $BaSO_4$ in the work of Hargreaves and Murray [33]. Apart from that, during fast pyrolysis in the activation of PKS at 800 °C and the gasification process from 800 °C to 1000 °C, it generates less surface area and forms larger mesopores and macropores due to water vapor elimination via hydration of unreacted H_2SO_4 [16, 54]. This was observed in the surface area of CAM-PKSdAC with 503 $m^2\ g^{-1}$ and has a large mesopores size of 33.65 nm when prepared using 10% H_2SO_4 mass loading and activation temperature of 700 °C, based on our parametric study [38]. A macropore will be created in its carbon structure by increasing the activation temperature above 700 °C [16, 54].

Consequently, heating $BaSO_4$ in the presence of air during CAM, the simultaneous activation and surface modification process was carried out at 400 °C and up to a maximum 700 °C to prevent rapid re-oxidation of BaS at 800–1100 °C that leads to larger mesopores formation [53]. In addition, given the Ba yield that did not significantly change with increasing reduction process time from 2 to 4 h [33], the CAM process of PKS was performed at the selected activation temperature of 2 h. Lastly, C7.5H$_2$SO$_4$-PKSdAC-700 resulted in a higher amount of Ba impregnated with 1.50 wt.% than C5H$_2$SO$_4$-PKSdAC-700 and C10H$_2$SO$_4$-PKSdAC-700, as shown in Fig. 1. This indicates that 7.5% H_2SO_4 mass loading has a higher potential to assist Ba impregnation on CAM-PKSdAC. By using H_2SO_4 mass loading of 7.5%, an adequate amount of $BaSO_4$ was generated with 10 wt.% $BaCl_2$ to initiate the reduction process with the carbon-reducing agent to BaS during the CAM thermal treatment process [30].

3.2 Statistical analysis of correlation and optimization study of CAM-PKSdAC synthesis

The amount of Ba impregnated in the 9 samples of CAM-PKSdAC from the correlation synthesis study in Section 2.3 was used to develop the regression model to determine the relationship of the independent variables with the dependent variable (response) as the impregnated Ba amount (wt.%). The model equation is as follows in Eq. 15:

$$\text{Impregnated Ba amount (wt.\%)} = +0.59 + 0.31A - 0.14B \\ + 0.44A^2 - 0.16B^2 + 0.010AB \tag{15}$$

where A is the activation temperature in °C and B is the H_2SO_4 mass loading in %.

The Analysis of Variance (ANOVA) of the correlation synthesis study for the impregnated Ba amount in CAM-PKSdACs is shown in Table 2. The model F-value of 38.54 implies that the overall model was significant with "Prob > F" value less than 0.05. Furthermore, the variables A, B, A^2, and B^2 were significant model terms. Among these four model terms, the result indicated that the activation temperature (A) was highly significant since its "Prob > F" value was less than 0.0001 (Prob > F < 0.05) with the highest F-value of 90.82, as shown in Table 2. This suggests activation temperature significantly affected the impregnated Ba amount in CAM-PKSdACs (response). "Adeq precision" measures the signal-to-noise ratio. A ratio of 18.695 indicates an adequate signal since a ratio greater than 4 is desirable. The standard deviation of the model was 0.080 for Eq. 15.

Figure 3 shows the variation of the experimental impregnated Ba amount to the predicted impregnated Ba amount. The predicted amount of impregnated Ba was close to the experimental values, indicating that the models developed were successful in correlating the CAM-PKSdAC preparation condition variables to the impregnated Ba amount. The coefficient of determination R^2 of 0.9649 indicates a strong correlation between the experimental and the predicted

Table 2 ANOVA for the selected design model for impregnated Ba amount in CAM-PKSdAC

Source	Sum of squares	DF	Mean square	F-value	Prob > F	Status
Model	1.22	5	0.24	38.54	< 0.0001	*Significant*
A	0.58	1	0.58	90.82	< 0.0001	
B	0.12	1	0.12	19.42	0.0031	
A^2	0.52	1	0.52	82.41	< 0.0001	
B^2	0.072	1	0.072	11.27	0.012	
AB	0.0004	1	0.0004	0.063	0.81	
Residual	0.044	7	0.0063			
Lack of Fit	0.044	3	0.015			
Cor total	1.27	13				
R-squared	0.9649					
Adj R-squared	0.9399					
Pred R-squared	0.6062					
Adeq precision	18.695					
Std. Dev	0.080					

Fig. 2 Effect of activation temperature on the amount of Ba impregnated in CAM-PKSdAC
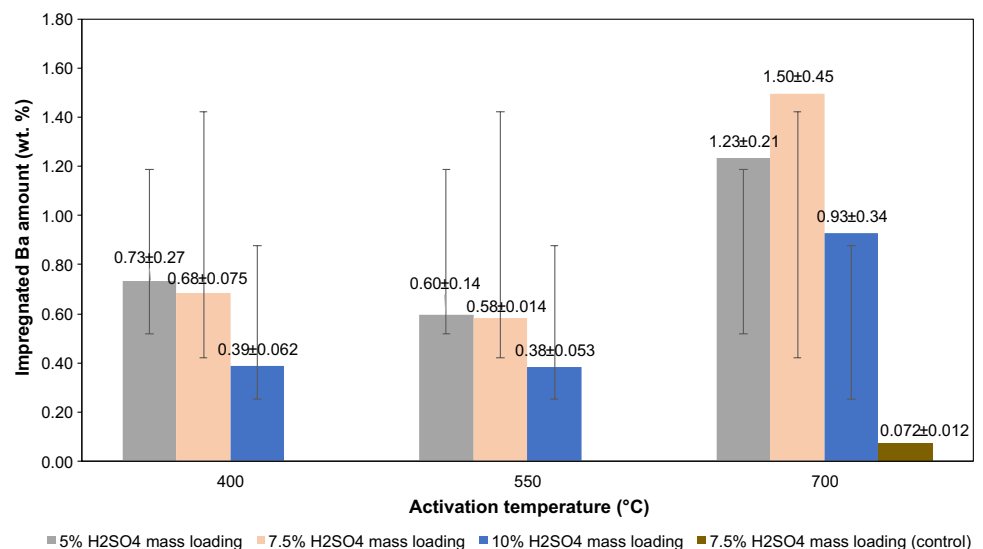
impregnated Ba amount from the models. The model also showed that R^2 reasonably agrees with the adjusted R^2 value of 0.9399 for the impregnated Ba amount, as shown in Table 2. However, from Table 2, the predicted R^2 value of 0.6062 is not as close to the adjusted R^2 indicating the effect of outliers in the regression model. Figure S2 plots residuals versus predicted impregnated Ba amount to estimate outliers and test the assumption of constant variance. In Figure S2, the results of the residuals are structureless. This manifests the assumption of homogeneity of variances for the activation temperature (A) and H_2SO_4 mass loading (B) on the impregnated Ba amount (response) in CAM-PKSdAC. The outliers are considered to have a value above 3 or below -3.

In a similar trend as Fig. 2, at 700 °C, the 3D surface plot in Fig. 4 showed that the impregnated Ba amount increased with decreasing H_2SO_4 mass loading (i.e., 10% to 7.5%), then decreased with a further decrease in H_2SO_4 mass

loading to 5%. The effect of activation temperature on the amount of Ba impregnated, as illustrated in Fig. 4, displayed the same trend as Fig. 2. At all three H_2SO_4 mass loading (5%, 7.5%, and 10%), the impregnated Ba amount showed a slight reduction of 18–29% when activation temperature increased from 400 °C to 550 °C and then improved with a further increase from 550 °C to 700 °C. Furthermore, Fig. 4 showed that at an activation temperature of 700 °C and 7.5% H_2SO_4 mass loading, the highest impregnated Ba amount exhibited by CAM-PKSdAC was 1.34 wt.% (denoted with red dots in Fig. 4). At below 400 °C or above 700 °C, H_2SO_4 mass loading of less than 5% or more than 10%, the impregnated Ba amount in CAM-PKSdAC increased in Fig. 4.

Therefore, the impregnation of Ba in CAM-PKSdAC was investigated beyond the CAM parameter ranges of H_2SO_4 mass loading of 4% and 11%, activation temperature of 338 °C and 762 °C. A full factorial CCD with a rotatability

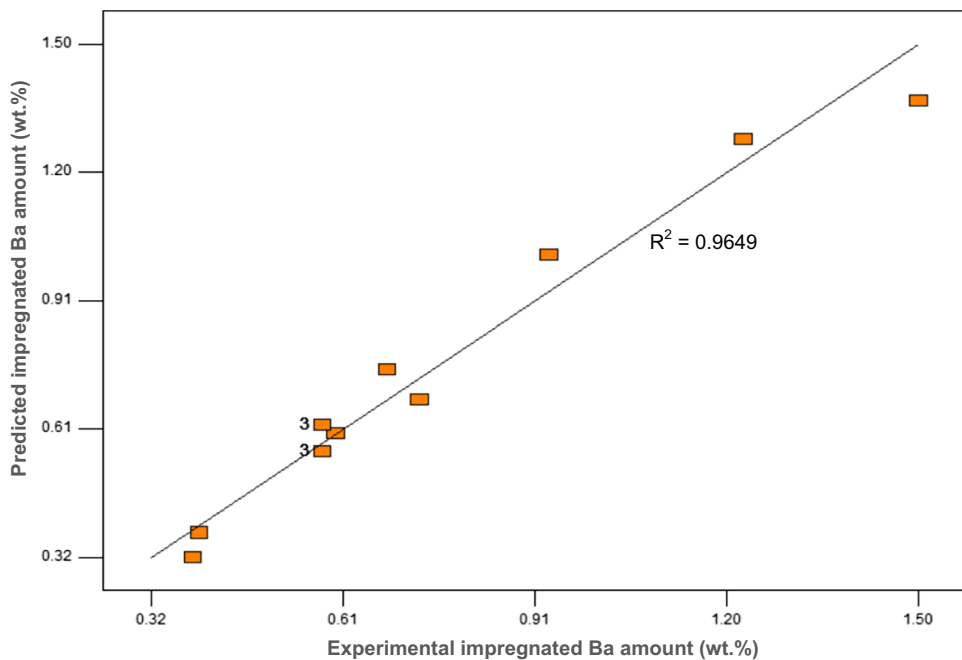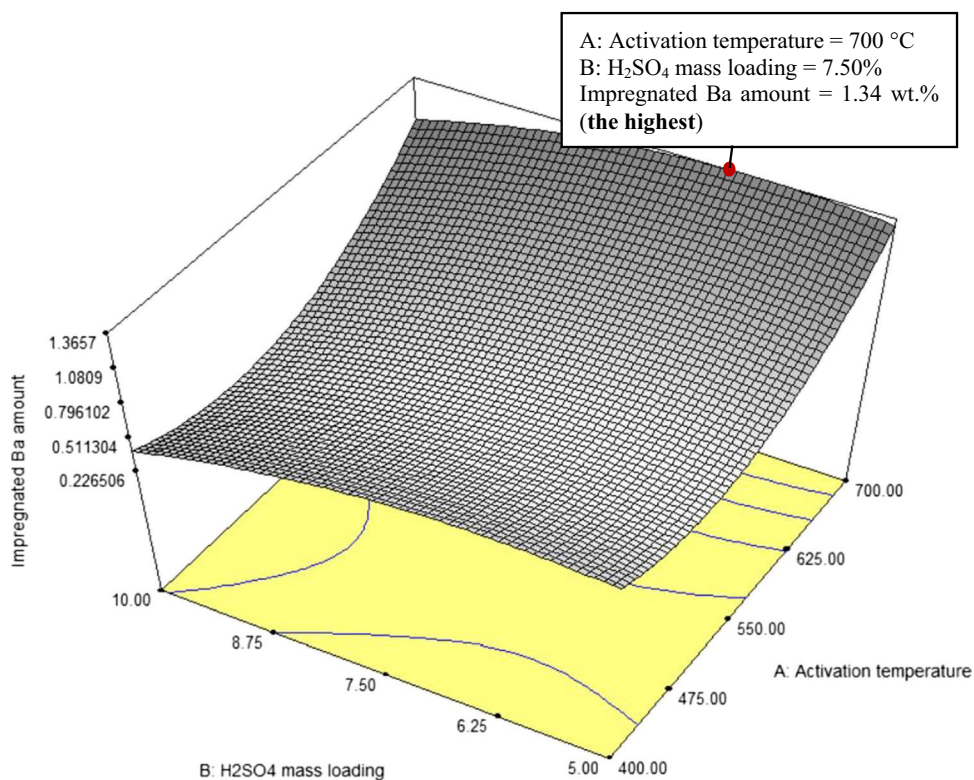**Fig. 3** Predicted versus experimental values of impregnated Ba amount in CAM-PKSdACs

Fig. 4 3D surface plot: activation temperature and H_2SO_4 mass loading effect on the impregnated Ba amount in CAM-PKSdACs at 10 wt.% $BaCl_2$ mass loading

A: Activation temperature = 700 °C
B: H_2SO_4 mass loading = 7.50%
Impregnated Ba amount = 1.34 wt.%
(**the highest**)

(α) of 1.414 was utilized to determine the possibility of achieving a high impregnated Ba amount. Both experimental and statistical analysis data for this investigation were presented in Supplementary Material as Table S2, Figure S3, Figure S4, and Figure S5. Tables S2(a) and (b) tabulate the experimental design and ANOVA for the selected design model for the regression model equation and coefficients of impregnated Ba amount in CAM-PKSdAC. In Table S2(b), activation temperature (Factor A) has a "Prob > F" value of 0.0005 (less than 0.05), indicating that it has a significant influence on the impregnated Ba amount in CAM-PKSdAC. The model found a high R^2 of 0.9131 ($R^2 > 0.90$), as shown

in Figure S3, indicating the variability in the response (impregnated Ba amount) could be attributed to the two factors (A: activation temperature and B: H_2SO_4 mass loading). The 3D plot in Figure S4 shows that the synthesis performed at an activation temperature of 700 °C at varying H_2SO_4 mass loading between 5 and 10% can impregnate a higher Ba amount in CAM-PKSdAC, which is in a similar trend as Fig. 4. The predicted impregnated Ba amount at 550 °C using 4% and 11% H_2SO_4 mass loading are denoted with blue dots, and brown dots indicated for the temperatures of 338 °C and 762 °C using 7.5% H_2SO_4 mass loading in Figure S4. At a temperature of 550 °C using 4% and 11% H_2SO_4 mass loading, CCD estimated an increase in impregnated Ba amount with 0.67 wt.% and 0.41 wt.% as observed in Fig. S4. While an increase in impregnated Ba amount of 0.67 wt.% was predicted at a lower temperature of 338 °C and 1.27 wt.% at a higher temperature of 762 °C when using 7.5% H_2SO_4 mass loading.

Based on the experimental design in Table S2(a), the synthesized CAM-PKSdAC data in Figure S5 indicates a decrease in impregnated Ba amount at the temperature of 338 °C and 762 °C using 7.5% H_2SO_4 mass loading with 0.67 wt.% and 1.14 wt.%, lower than at 400 °C (0.68 wt.% Ba) and 700 °C (1.50 wt.% Ba). Under an activation temperature of 550 °C, the CAM-PKSdAC prepared using 4% H_2SO_4 mass loading has decreased impregnated Ba amount of 0.51 wt.% compared to CAM-PKSdAC prepared by 5% H_2SO_4 mass loading (0.60 wt.%). Further increasing the H_2SO_4 mass loading to 11% only slightly increased the impregnated Ba amount to 0.44 wt.% than 10% H_2SO_4 mass loading with 0.38 wt.%. This has no significant influence since activation temperature was the main factor affecting Ba impregnation, as determined in Table S2(b) and Table 2 from the correlation and optimization study. In summary, the optimal conditions to prepare PKSdAC via the CAM process obtained from the correlation and optimization study were 7.5% H_2SO_4 mass loading and an activation temperature of 700 °C. The optimal CAM parameters were used to perform the validation of the model in the following section.

3.3 Model validation

The statistical analysis of the Design-Expert software gave one numerical solution of optimum CAM process conditions with a desirability value of 0.925 for the production of CAM-PKSdAC based on the maximum impregnated Ba amount. The optimum conditions were determined numerically: activation temperature of 700 °C and H_2SO_4 mass loading of 7.5%, as shown in Table 3. The maximum impregnated Ba of 1.34 wt.% was predicted at this synthesis condition. The verification test was conducted to synthesize CAM-PKSdAC under the optimum synthesis conditions to validate the model's accuracy. The verification test resulted

Table 3 Model validation

Activation temperature, A (°C)	H_2SO_4 mass loading, B (%)	Impregnated Ba amount (wt.%)		Percentage error (%)
		Predicted from model	Experimental	
700	7.5	1.34	1.50	11.94

Table 4 Effect of $BaCl_2$ mass loading on the impregnated Ba amount in the CAM-PKSdAC

Sample	$BaCl_2$ mass loading (wt.%)	Impregnated Ba amount (wt.%)
C7.5H$_2$SO$_4$-PKSdAC-700-2BaCl$_2$	2	0.088
C7.5H$_2$SO$_4$-PKSdAC-700-4BaCl$_2$	4	0.19
C7.5H$_2$SO$_4$-PKSdAC-700-6BaCl$_2$	6	0.26
C7.5H$_2$SO$_4$-PKSdAC-700-8BaCl$_2$	8	0.68
C7.5H$_2$SO$_4$-PKSdAC-700-10BaCl$_2$	10	1.50

in an impregnated Ba amount of 1.50 wt.% with a standard deviation of 0.45, as reported in Table 3. The experimental value for impregnated Ba amount agrees with the predicted value, with errors of 11.94%.

3.4 Effect of $BaCl_2$ mass loading on CAM-PKSdAC

The ICP-OES analysis results for the impregnated Ba amount in 5 samples of CAM-PKSdAC prepared at varying $BaCl_2$ mass loading of 2–10 wt.% is demonstrated in Table 4. Table 4 shows that increasing the $BaCl_2$ mass loading increases the impregnated Ba amount, indicating the impregnation of Ba metal was favourable when the $BaCl_2$ mass loading increases until 10 wt.%. The addition of 10 wt.% $BaCl_2$ resulted in the highest amount of Ba impregnated in CAM-PKSdAC with 1.50 wt.%. This result also shows lower $BaCl_2$ mass loading did not achieve a comparable impregnated Ba amount to 10 wt.% $BaCl_2$ mass loading. The $BaCl_2$ mass loading beyond 10 wt.% could seal AC's pores and generates macropore, which is not desirable for the adsorption of CO_2 [55].

H_2SO_4 reacted with increasing $BaCl_2$ loading during the chemical impregnation to produce an increasing amount of $BaSO_4$ based on the reaction stoichiometry (i.e., $BaCl_2 + H_2SO_4 \rightarrow BaSO_4 + 2HCl$ [Eq. 1]). In the experiment with 7.5% H_2SO_4 mass loading, $BaCl_2$ is the limiting reactant, and H_2SO_4 is the excess reactant. The actual experimental and theoretical amounts of $BaCl_2$, $BaSO_4$, and the impregnated Ba amount are presented in Tables S3 and S4. Table S3 shows a constant step increase of impregnated Ba with the increase in $BaCl_2$ mass loading. The actual experimental impregnated Ba in Table S4 shows an exponential

trend, indicating a second-order reaction. Therefore, a further increase in $BaCl_2$ mass loading will not return a significant cost-effective improvement. Based on the actual Ba impregnation, only 1.37–4.74 wt.% $BaCl_2$ out of total $BaCl_2$ given (2–10 wt.%) was consumed with 0.0063–0.11 g H_2SO_4 penetrated beneath the surface of CAM-PKSdAC in the precipitation reaction. During chemical impregnation with 7.5% H_2SO_4 mass loading, a fixed amount of H_2SO_4 was impregnated on the surface of CAM-PKSdAC, and excess H_2SO_4 was removed by filtration. The drying process did not evaporate the H_2SO_4 since the boiling point of H_2SO_4 was 335 °C [56]. Therefore, the actual impregnated Ba depends on the amount of impregnated H_2SO_4. This resulted in 0.015–0.25 g $BaSO_4$ obtained via $BaCl_2$ impregnation, which was reduced to BaS during CAM to produce 0.088–1.50 wt.% impregnated Ba amount.

A higher amount of $BaSO_4$ crystals generated more reduction to BaS, which penetrated the porous structure of CAM-PKSdAC and entrapped into the micropores during
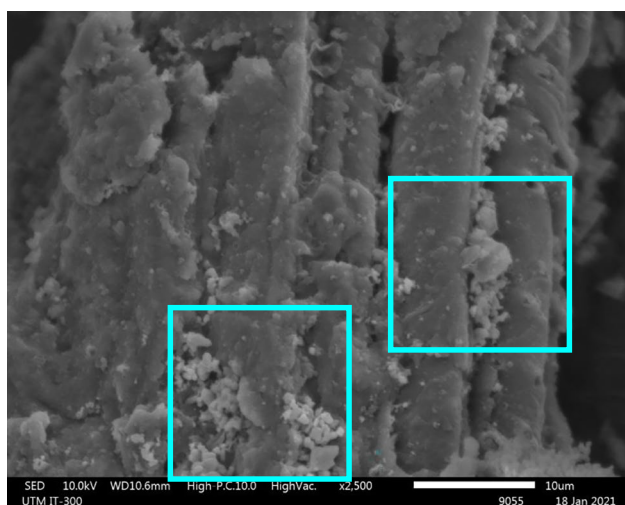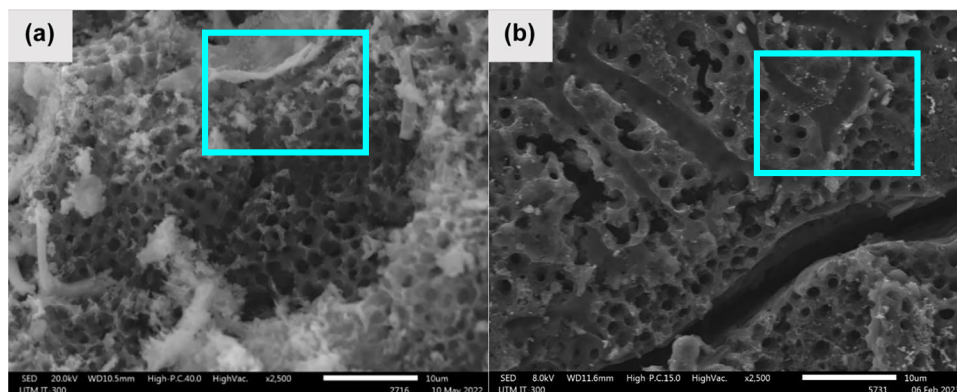

Fig. 5 SEM images of CAM-PKSdAC (C10H$_2$SO$_4$-PKSdAC-700) with magnification factors of 2,500 (Reproduced from [38])

the activation process at high temperatures [55]. Based on our parametric study [38], the SEM micrograph (Fig. 5) showed the addition of 10 wt.% $BaCl_2$ causes the interior pores of CAM-PKSdAC to be occupied with an abundance of $BaSO_4$ (denoted with a blue box). By further increasing the addition of $BaCl_2$ to 20 wt.%, Kim et al. [51] reported that high Ba loading (20 wt.%) resulted in the formation of more $BaSO_4$ into the interior Pt-BaO/Al$_2$O$_3$ sample. After high temperature desulphation, the residual sulphur exists as large BaS particles [51]. This hinders the diffusion of Ba species into the interior region of Pt-BaO/Al$_2$O$_3$ [51]. Compared to the Pt-BaO/Al$_2$O$_3$ sample prepared with 8 wt.% Ba, a "monolayer" $BaSO_4$ species experienced a complete desulphation at lower temperatures compared to when more $BaSO_4$ was produced at high Ba loading [51].

In addition, the aim of studying the effect of $BaCl_2$ mass loading was to investigate the possibility of reducing the surface modification agent required. Hence, the experiments did not include $BaCl_2$ mass loading than 10 wt.%. The optimum process conditions for the CAM process parameters examined in this work were H_2SO_4 mass loading of 7.5%, activation temperature of 700 °C, and $BaCl_2$ mass loading of 10 wt.%. The optimum CAM-PKSdAC was used to characterize its surface area, pore structure, morphology, and chemical elements.

3.5 Optimized CAM-PKSdAC characterization

The surface morphology of the optimum CAM-PKSdAC (C7.5H$_2$SO$_4$-PKSdAC-700) and conventional surface modified-activated PKSdAC prepared via 2-step H_2SO_4 activation followed by the subsequent $BaCl_2$ modification at an activation temperature of 700 °C and 7.5% H_2SO_4 (C7.5H$_2$SO$_4$-PKSdAC-700-modified) are shown in Fig. 6(a) and (b). The optimum CAM-PKSdAC displays a sponge-like structure with the presence of $BaSO_4$ metal salts (white crystalline material) on its external surface and in its internal pore structure (denoted with a blue box) in Fig. 6(a). Compared to conventional surface modified-activated PKSdAC, it has

Fig. 6 SEM image of (**a**) CAM-PKSdAC (C7.5H$_2$SO$_4$-PKSdAC-700) and (**b**) conventional surface modified-activated PKSdAC (C7.5H$_2$SO$_4$-PKSdAC-700-modified) with a magnification factor of 2500x

a porous structure and a crack surface containing a small amount of BaSO$_4$ metal salts on its surface and interior pores, as shown in Fig. 6(b).

The FTIR spectra of the optimum CAM-PKSdAC and conventional surface modified-activated PKSdAC over the range of 400–4000 cm^{-1} are presented in Fig. 7. In the FTIR spectra of optimum CAM-PKSdAC (Fig. 7(a)), the observed

wavenumbers are 729.01, 1026.02, 1164.88, 1463.81, 1741.53, 2860.13, and 2925.70 cm^{-1}. The spectrum peaks at 729.01, 1026.02, and 1164.88 cm^{-1} were assigned to C-H bending vibrations [57]. The C-O stretch of carbon, hydrogen and SO$_2$ (O=S=O) stretching from H$_2$SO$_4$ species appeared at 1164.88 cm^{-1} for the optimum CAM-PKSdAC [58, 59]. The alkyl C=C bending from the optimum
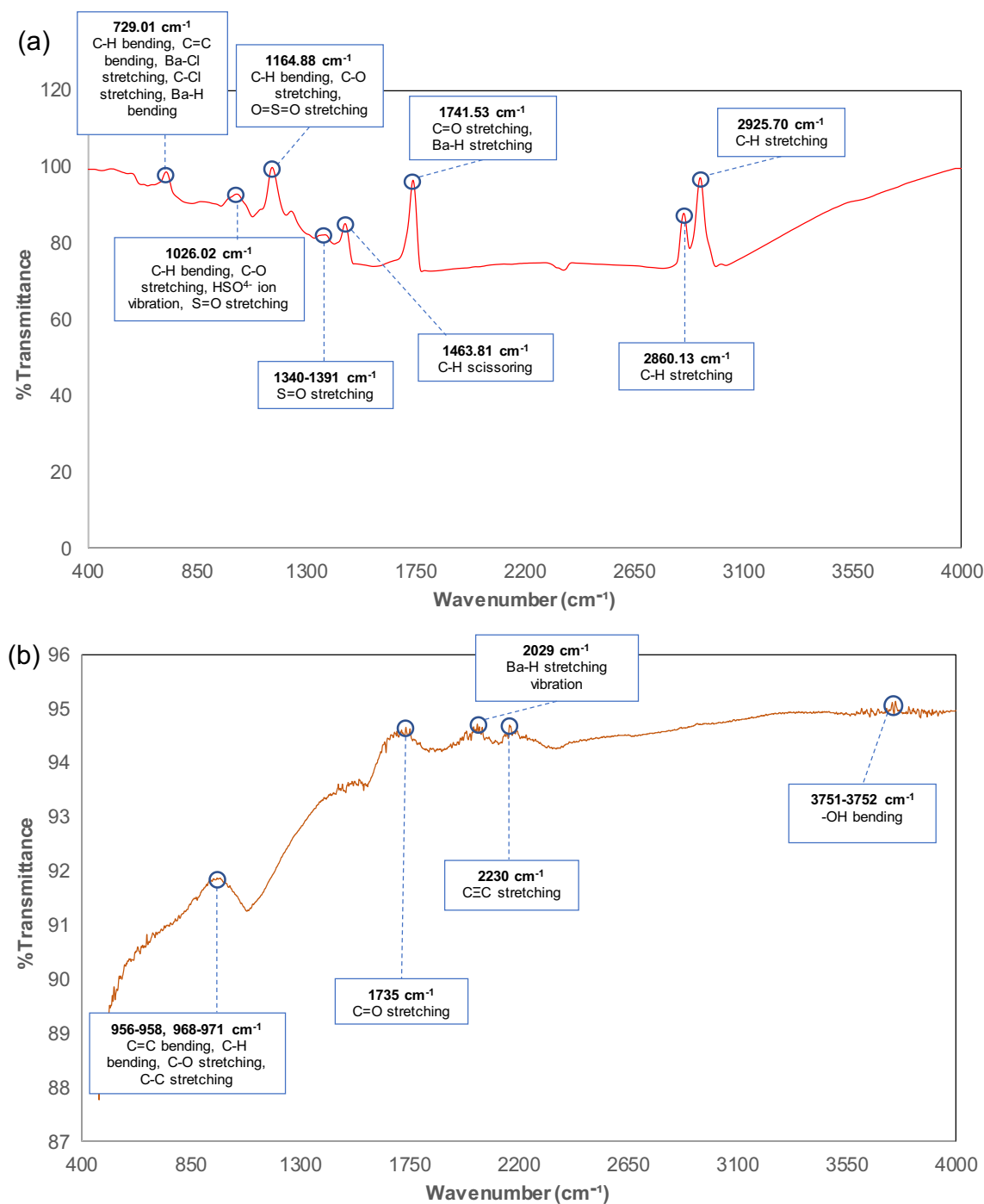
Fig. 7 FTIR spectra of (**a**) optimum CAM-PKSdAC (C7.5H$_2$SO$_4$-PKSdAC-700) and (**b**) conventional surface modified-activated PKSdAC (C7.5H$_2$SO$_4$-PKSdAC-700-modified)

CAM-PKSdAC and Ba metal-Cl stretching were presented at a weak peak of 729.01 cm^{-1} [57, 59]. The carbonyl (C-O) stretch of carbon and hydrogen, HSO$_4^{4-}$ ion vibration, and S=O (sulphur and oxygen) stretching of inorganic sulphates appeared as a weak peak at 1026.02 cm^{-1} [57–59]. In contrast, carboxylic acid's carbonyl (C=O) stretch is a strong peak at 1741.53 cm^{-1} [57, 59]. Another high-intensity peak was observed at 2925.70 cm^{-1}, along with the broad shoulder-type peak around 2860.13 cm^{-1}; these were associated with the alkyl C-H stretching [57, 59].

The spectrum peaks at 729.01 cm^{-1} and 1463.81 cm^{-1} from the optimum CAM-PKSdAC sample show the presence of C–Cl stretching and C-H scissoring, respectively [57, 59]. A spectrum peak between 500–1500 cm^{-1} was associated with the presence of BaSO$_4$ compound in the optimum CAM-PKSdAC [57]. The Ba metal-H stretching and Ba metal-H bending appeared as a strong peak at 1741.53 cm^{-1} and a weak peak at 729.01 cm^{-1} [57]. In addition, the stretching of S=O from sulphate was observed at the peak region between 1340–1391 cm^{-1} [59]. Therefore, impregnation of Ba metal salt was effectively performed onto the PKSdAC through the CAM process using H$_2$SO$_4$ as activating agent and BaCl$_2$ for metal functionalization. In the FTIR spectra of the conventional surface modified-activated PKSdAC shown in Fig. 7(b), the sharp peak at 3751–3752 cm^{-1} was due to the bending of -OH group from the H$_2$O molecules chemisorbed onto the surface of conventional surface modified-activated PKSdAC when exposed to the atmosphere [57]. The peak at 2029 cm^{-1} was associated with the stretching vibration of the Ba-H molecule, while those at 1735 and 2230 cm^{-1} were related to the stretching of alkyne (C≡C) and C=O groups [57, 59]. The C≡C group was formed by eliminating a hydrogen and a halogen (Cl) atom [60]. In addition, a very weak peak corresponding to the alkyl C=C and C-H bending, carbonyl (C-O) stretch of carbon and hydrogen, and carbon atoms (C–C) stretching vibration were visible around 956–958 cm^{-1} and 968–971 cm^{-1} [57, 59].

The elemental analysis of raw PKS and optimum CAM-PKSdAC are summarized in Table 5. The untreated palm kernel shell contains 47.69 wt.% carbon, 5.32 wt.% hydrogen, and 0.17 wt.% nitrogen contents with negligible sulphur detection. The raw PKS's elemental composition was within other research work's reported range but slightly lower, as presented in Table 5. After the CAM process, the carbon content increased from 47.69 wt.% to 71.88 wt.%, while the hydrogen content decreased from 5.32 wt.% to 1.70 wt.%. This behaviour was due to the removal of volatile matter during the CAM process, which subsequently caused an increase in carbon content and reduced hydrogen content. As mentioned earlier, BaSO$_4$ was produced from the impregnation of BaCl$_2$ onto the H$_2$SO$_4$-treated PKS. During the thermal CAM process, BaS is generated from the reduction of BaSO$_4$ in the presence of carbon as the reducing agent. This eventually caused an increase in sulphur content from 0 wt.% in palm kernel shell to 0.044 wt.% in optimum CAM-PKSdAC. The use of carbon in the reduction of BaSO$_4$ attributed to the lower carbon content in optimum CAM-PKSdAC than the conventional surface modified-activated PKSdAC prepared via 2-step H$_2$SO$_4$ activation followed by the subsequent BaCl$_2$ modification at the optimal condition and other research works in Table 5. The nitrogen content remained almost unchanged during the CAM process, indicating the presence of nitrogen naturally in the aromatic structure of the optimum CAM-PKSdAC and not in functional groups on the layer edges [61]. The oxygen compound decreases from 46.82 wt.% to 26.01 wt.%, manifesting the loss of oxygen-functional groups

Table 5 Comparison of elemental analysis of raw PKS and CAM-PKSdAC prepared via CAM by H$_2$SO$_4$ activation and BaCl$_2$ functionalization under optimum conditions with others' work

Sample	C (wt.%)	H (wt.%)	N (wt.%)	S (wt.%)	*O (wt.%)	References
Raw precursor						
PKS	47.69	5.32	0.17	0.00	46.82	This study
PKS	47.77–50.12	5.98–7.45	0.90–3.32	0.00–0.089	39.15–45.31	[54, 62–65]
Derived activated carbon						
CAM-PKSdAC (C7.5H$_2$SO$_4$-PKSdAC-700)	71.88	1.70	0.37	0.044	26.01	This study
Conventional surface modified-activated PKSdAC (C7.5H$_2$SO$_4$-PKSdAC-700-modified)	84.90	0.95	0.34	0.00	13.80	This study
PKSdAC by H$_2$SO$_4$ activation	83.30	0.40	0.20	-	16.10	[16]
PKSdAC by KOH activation	84.10	0.80	0.60	-	14.50	[66]
PKSdAC by H$_2$SO$_4$ activation	83.30	0.40	0.20	-	16.10	[66]
PKSdAC by ZnCl$_2$ activation	81.84	2.50	0.51	-	15.05	[67]
PKSdAC by H$_3$PO$_4$ activation	72.90	2.30	0.70	-	24.10	[68]

*Oxygen content was calculated by difference (i.e., 100-(C+H+N+S))

Table 6 The textural properties of CAM-PKSdAC and conventional surface modified-activated PKSdAC prepared under optimum conditions

Sample	S_{BET} (m^2 g^{-1})	V_{total} (cm^3 g^{-1})	V_{micro} (cm^3 g^{-1})	D_{avg} (nm)
Mesoporous CAM-PKSdAC (C7.5H$_2$SO$_4$-PKSdAC-700 mesopores)	423.00	0.19	0.14	1.78
Microporous CAM-PKSdAC (C7.5H$_2$SO$_4$-PKSdAC-700 micropores)	420.00	0.19	0.14	1.78
Conventional surface modified-activated PKSdAC (C7.5H$_2$SO$_4$-PKSdAC-700-modified)	565.00	0.18	0.18	1.27
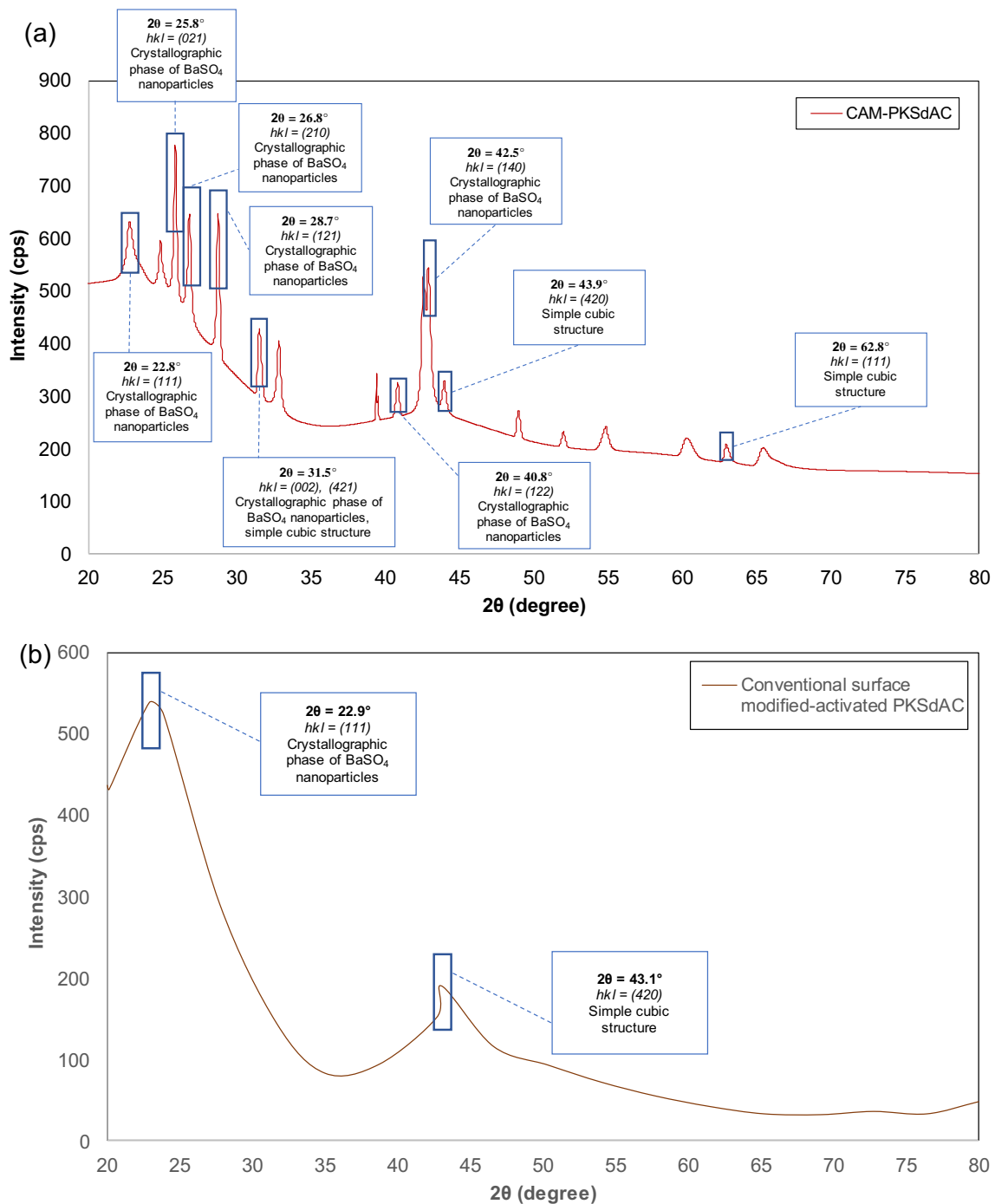
Fig. 8 XRD pattern for the (**a**) optimum CAM-PKSdAC and (**b**) conventional surface modified-activated PKSdAC

during the thermal CAM process. The conventional surface modified-activated PKSdAC has the highest carbon content of 84.90 wt.%, a decreased hydrogen and oxygen content with 0.95 wt.% and 13.80 wt.%, 0 wt.% sulphur content, and a similar nitrogen content of 0.34 wt.% in comparison with CAM-PKSdAC. The $BaCl_2$ modification after the H_2SO_4 activation does not significantly impregnate Ba on the PKSdAC surface and its interior pores.

The textural properties of the optimum CAM-PKSdAC analyzed from the N_2 adsorption/desorption isotherms analysis indicated type I(b) adsorption isotherm with hysteresis loop of type H4 for both micropore and mesopore structures according to the IUPAC classification [43]. This shows a pore size distribution in the micropore range with some mesopores [43]. Table 6 summarizes the BET surface area (S_{BET}), total pore volume (V_{total}), micropore volume (V_{micro}), and average pore diameter (D_{avg}) for the optimum CAM-PKSdAC. The micropore structure has a surface area of 420.00 m^2 g^{-1}, V_{total} of 0.19 cm^3 g^{-1}, V_{micro} of 0.14 cm^3 g^{-1}, and D_{avg} of 1.78 nm. In comparison, the mesopore structure possessed comparable surface area (423.00 m^2 g^{-1}), V_{total} (0.19 cm^3 g^{-1}), V_{micro} (0.14 cm^3 g^{-1}), and D_{avg} (1.78 nm). The pore size distribution using the N_2 adsorption data at 77 K discovered that the micropore and mesopore structures consist of the 3.03–3.23 nm mesopores. The incorporation of Ba forms these pores into the carbon structure of optimum CAM-PKSdAC during $BaSO_4$ reduction, and therefore, causes the surface area to decrease. The conventional surface modified-activated PKSdAC has a higher S_{BET} of 565.00 m^2 g^{-1} compared to the optimum CAM-PKSdAC with V_{total} of 0.18 cm^3 g^{-1}, V_{micro} of 0.18 cm^3 g^{-1}, and D_{avg} of 1.27 nm. The N_2 adsorption/desorption isotherms analysis indicated type I adsorption isotherm with hysteresis loop of type H4 for conventional surface modified-activated PKSdAC, showing it is a microporous material with slight mesoporous characteristic [43].

Figure 8 presents the XRD pattern for the optimum CAM-PKSdAC and conventional surface modified-activated PKSdAC. The XRD spectra for the optimum CAM-PKSdAC shown in Fig. 8(a) were collected in the scan range 2θ from 5° to 90° at a scan rate of 0.12 sec step^{-1}. The broadened peaks of a crystallographic phase of $BaSO_4$ nanoparticles were observed at 22.8° (111), 25.8° (021), 26.8° (210), 28.7° (121), 31.5° (002), 40.8° (122), and 42.5° (140) (2θ). This indicates that $BaSO_4$ crystals were encapsulated in the optimum CAM-PKSdAC, which aligned with the observation from the XRD pattern for as-synthesized $BaSO_4$ nanoparticles [69]. A simple cubic carbon structure was exhibited in the optimum CAM-PKSdAC by showing broadened peaks at 31.5° (421), 43.9° (420), and 62.8° (111) in Fig. 8(a). In the XRD spectra for conventional surface modified-activated PKSdAC shown in Fig. 8(b), the peak at 22.9° (111) and 43.1° (420) were associated with the presence

of crystallographic phase of $BaSO_4$ nanoparticles in its simple cubic carbon structure.

4 Conclusion

A concurrent activation and surface modification (CAM) process was developed and successfully synthesized palm kernel shell-derived activated carbon (PKSdAC) impregnated with Ba. The optimum process conditions for the CAM process in producing PKSdAC were H_2SO_4 mass loading of 7.5%, activation temperature of 700 °C, and $BaCl_2$ mass loading of 10 wt.%. The impregnated Ba amount predicted from the statistical analysis (1.34 wt.%) agreed with the Ba amount obtained from the verification test (1.50 wt.%) under the same optimum process conditions with a percentage error of 11.94% in the measurement. The PKSdAC prepared from optimum CAM process conditions exhibited a sponge-like simple cubic carbon structure encapsulated with $BaSO_4$ crystals with a surface area of 420.00 m^2 g^{-1} and 423.00 m^2 g^{-1} for its micropore and mesopore structure. The CAM-PKSdAC obtained a total pore volume of 0.19 cm^3 g^{-1}, a micropore volume of 0.14 cm^3 g^{-1}, and an average pore diameter of 1.78 nm. The $BaCl_2$ modification after the H_2SO_4 activation does not significantly impregnate Ba in the PKSdAC, indicating the simplified scheme of a 2-step integrated CAM process is viable to impregnate high Ba in the PKSdAC with similar textural structure compared to the conventional 2-steps H_2SO_4 activation followed by the subsequent $BaCl_2$ modification. Through this study, the surface modification process can simultaneously be conducted with chemical activation on PKS to introduce chemical groups or charges on the surface. The work presented will serve as a cross-reference in future studies of new PKSdAC synthesis and surface modification technologies. This study also uncovers critical insights into using barium salts in PKSdAC production.

Authors' contributions Jia Yen Lai: Conceptualization, Data curation, Formal analysis, Investigation, Methodology, Software, Validation,

Data availability The datasets generated during and/or analysed during the current study are available in the Supplementary Materials and in the main manuscript.

Declarations

Ethical approval Not applicable.

Competing interests On behalf of all authors, the corresponding author declares that there are no competing interests of a financial or personal nature.

References

1. Ahmad AL, Loh MM, Aziz JA (2007) Preparation and characterization of activated carbon from oil palm wood and its evaluation on methylene blue adsorption. Dyes Pigm 75(2):263–272
2. González-Navarro MF, Giraldo L, Moreno-Piraján JC (2014) Preparation and characterization of activated carbon for hydrogen storage from waste African oil-palm by microwave-induced LiOH basic activation. J Anal Appl Pyrolysis 107:82–86
3. Hamad BK, Noor AM, Afida AR, Mohd Asri MN (2010) High removal of 4-chloroguaiacol by high surface area of oil palm shell-activated carbon activated with NaOH from aqueous solution. Desalination 257(1):1–7
4. Wahi R, Ngaini Z, Usun Jok V (2009) Removal of mercury, lead and copper from aqueous solution by activated carbon of palm oil empty fruit bunch. World Appl Sci J 5:84–91
5. Foo KY, Hameed BH (2011) Preparation of oil palm (Elaeis) empty fruit bunch activated carbon by microwave-assisted KOH activation for the adsorption of methylene blue. Desalination 275(1):302–305
6. Guo J, Lua AC (2002) Microporous activated carbons prepared from palm shell by thermal activation and their application to sulfur dioxide adsorption. J Colloid Interface Sci 251(2):242–247
7. Jia QP, Lua AC (2008) Effects of pyrolysis conditions on the physical characteristics of oil-palm-shell activated carbons used in aqueous phase phenol adsorption. J Anal Appl Pyrolysis 83(2):175–179
8. Sohni S, Norulaini NAN, Hashim R, Khan SB, Fadhullah W, Mohd Omar AK (2018) Physicochemical characterization of Malaysian crop and agro-industrial biomass residues as renewable energy resources. Ind Crop Prod 111:642–650
9. Rafatullah M, Ahmad T, Ghazali A, Sulaiman O, Danish M, Hashim R (2013) Oil palm biomass as a precursor of activated carbons: A review. Crit Rev Env Sci Technol 43(11):1117–1161
10. Hoseinzadeh Hesas R, Arami-Niya A, Wan Daud WMA, Sahu J (2015) Microwave-assisted production of activated carbons from oil palm shell in the presence of CO_2 or N_2 for CO_2 adsorption. J Ind Eng Chem 24:196–205
11. Rodríguez-Reinoso F, Molina-Sabio M (1992) Activated carbons from lignocellulosic materials by chemical and/or physical activation: An overview. Carbon 30(7):1111–1118
12. Rashidi NA, Yusup S (2016) An overview of activated carbons utilization for the post-combustion carbon dioxide capture. J CO_2 Util 13:1–16
13. Rashidi NA, Yusup S (2017) A review on recent technological advancement in the activated carbon production from oil palm wastes. Chem Eng J 314:277–290
14. Lai JY, Ngu LH (2020) The production cost analysis of oil palm waste activated carbon: a pilot-scale evaluation. Greenh Gases Sci Technol 10(5):999–1026
15. Lai JY, Ngu LH, Hashim SS, Chew JJ, Sunarso J (2021) Review of oil palm-derived activated carbon for CO_2 capture. Carbon Lett 31(2):201–252
16. Guo J, Xu WS, Chen YL, Lua AC (2005) Adsorption of NH_3 onto activated carbon prepared from palm shells impregnated with H_2SO_4. J Colloid Interface Sci 281(2):285–290
17. Guo J, Lua AC (2003) Textural and chemical properties of adsorbent prepared from palm shell by phosphoric acid activation. Mater Chem Phys 80(1):114–119
18. Tian DQ, Xu ZH, Zhang DF, Chen WF, Cai JL, Deng HX, Sun ZH, Zhou YW (2019) Micro–mesoporous carbon from cotton waste activated by $FeCl_3$/$ZnCl_2$: Preparation, optimization, characterization and adsorption of methylene blue and eriochrome black T. J Solid State Chem 269:580–587
19. Sun YY, Yue QY, Mao YP, Gao BY, Gao Y, Huang LH (2014) Enhanced adsorption of chromium onto activated carbon by microwave-assisted H_3PO_4 mixed with Fe/Al/Mn activation. J Hazard Mater 265:191–200
20. Amuda OS, Ibrahim AO (2006) Industrial wastewater treatment using natural material as adsorbent. Afr J Biotechnol 5(16):1483–1487
21. Ajani AO, Dada EO, Olu-arotiowa OA, Okeowo I (2019) Adsorption of methylene blue from aqueous solution using microwave-assisted $BaCl_2$ modified activated carbon produced from mango seed shell. LAUJOCES 3(1):72–82
22. Khalil SH, Aroua MK, Daud WMAW (2012) Study on the improvement of the capacity of amine-impregnated commercial activated carbon beds for CO_2 adsorbing. Chem Eng J 183:15–20
23. Aroua M, Daud W, Yin C, Adinata D (2008) Adsorption capacities of carbon dioxide, oxygen, nitrogen and methane on carbon molecular basket derived from polyethyleneimine impregnation on microporous palm shell activated carbon. Sep Purif Technol 62(3):609–613
24. Hidayu ARN, Muda N (2017) Impregnated palm kernel shell activated carbon for CO_2 adsorption by pressure swing adsorption. Indian J Sci Technol 10(2):1–6
25. Hidayu AR, Muda N (2016) Preparation and characterization of impregnated activated carbon from palm kernel shell and coconut shell for CO_2 capture. Procedia Eng 148:106–113
26. Park HJ, Suh MP (2013) Enhanced isosteric heat, selectivity, and uptake capacity of CO_2 adsorption in a metal-organic framework by impregnated metal ions. Chem Sci 4(2):685–690

27. Lai JY, Ngu LH (2022) Techno-economic feasibility study for concurrent activated and modified palm kernel shell–derived activated carbon. Biomass Convers Biorefin: 1–12 Part of a collection: Biomass for Energy and Value-added Products – Technological Progress 2022. https://doi.org/10.1007/s13399-022-03520-y

28. Liu Z, Green WH (2013) Experimental investigation of sorbent for warm CO_2 capture by pressure swing adsorption. Ind Eng Chem Res 52(28):9665–9673

29. Kim BJ, Cho KS, Park SJ (2010) Copper oxide-decorated porous carbons for carbon dioxide adsorption behaviors. J Colloid Interface Sci 342(2):575–578

30. Balintova M, Demcak S, Estokova A, Holub M, Pavlikova P (2017) Study of thermal reduction of barium sulphate for barium sulphide preparation. In: Environmental Engineering. Proceedings of the International Conference on Environmental Engineering (ICEE), vol 10. Vilnius Gediminas Technical University, Department of Construction Economics & Property, pp 1–6

31. Budnikov P, Ginstling AM (1968) Principles of solid state chemistry: Reactions in solids. Mclaren, Croydon, UK

32. Murthy JSN, Reddy PVV (2012) Solid-state reaction between barium sulfate and carbon. Chem Eng Commun 199(8):966–990

33. Hargreaves K, Murray DM (1989) Factors influencing the reduction of barium sulphate. J Chem Technol Biotechnol 45(4):319–325

34. Herschel WH (1926) Manufacture of barium sulphide. Chem Ztg 50:692–693

35. Lewandowski WM, Ryms M, Kosakowski W (2020) Thermal biomass conversion: A review. Processes 8(5):1–45

36. Lin YT, Li YR, Xu ZC, Guo JX, Zhu TY (2021) Carbon consumption and adsorption-regeneration of H_2S on activated carbon for coke oven flue gas purification. Environ Sci Pollut Res 28(43):60557–60568

37. Li YR, Lin YT, Wang B, Ding S, Qi F, Zhu TY (2019) Carbon consumption of activated coke in the thermal regeneration process for flue gas desulfurization and denitrification. J Clean Prod 228:1391–1400

38. Lai JY, Ngu LH, Chew JJ, Khaerudini DS (2022) Parametric study of concurrent activation and surface modification (CAM) process for palm kernel shell derived activated carbon. Chem Eng Trans 97:415–420

39. Baş D, Boyacı İH (2007) Modeling and optimization I: Usability of response surface methodology. J Food Eng 78(3):836–845

40. National Institute of Standards and Technology (NIST) 2023, 5.3.3.6.1. Central Composite Designs (CCD), U.S. Department of Commerce, viewed 2 September 2023, https://www.itl.nist.gov/div898/handbook/pri/section3/pri3361.htm

41. Epa US (1996) Method 6010B: Inductively coupled plasma-atomic emission spectrometry. DC, Revision, Washington, p 2

42. Epa US (1996) Method 3050B: Acid digestion of sediments, sludges, and soils. DC, Revision, Washington, p 2

43. Thommes M, Kaneko K, Neimark AV, Olivier JP, Rodriguez-Reinoso F, Rouquerol J, Sing KSW (2015) Physisorption of gases, with special reference to the evaluation of surface area and pore size distribution (IUPAC Technical Report). Pure Appl Chem 87(9–10):1051–1069

44. Lowell S, Shields JE, Thomas MA, Thommes M (2006) Characterization of porous solids and powders: Surface area, pore size and density (vol 16). Springer Science & Business Media

45. Rouquerol J, Rouquerol F, Sing K (1998) Adsorption by Powders and Porous Solids: Principles. Elsevier Science, Methodology and Applications

46. Sherwood PMA (2001) Carbons and Graphites: Surface Properties of. In: Buschow KHJ, Cahn RW, Flemings MC, Ilschner B, Kramer EJ, Mahajan S, Veyssière P (eds) Encyclopedia of Materials: Science and Technology. Elsevier, Oxford, pp 985–995

47. Anderson JM, Voskerician G (2010) 14 - The challenge of biocompatibility evaluation of biocomposites. In: Ambrosio L (ed) Biomedical Composites. Woodhead Publishing, pp 325–353

48. Sharma RK, Wooten JB, Baliga VL, Martoglio-Smith PA, Hajaligol MR (2002) Characterization of char from the pyrolysis of tobacco. J Agric Food Chem 50(4):771–783

49. Zhang HY, Cheng YT, Vispute TP, Xiao R, Huber GW (2011) Catalytic conversion of biomass-derived feedstocks into olefins and aromatics with ZSM-5: the hydrogen to carbon effective ratio. Energy Environ Sci 4(6):2297–2307

50. Ivanto G, Fatra F, Dera NS, Muryanto S, Bayuseno AP (2017) Citric acid addition to controlling crystallization of barium sulphate ($BaSO_4$) in pipes through Ba^{2+} concentration variation in the solution. IOP Conf Ser Mater Sci Eng 202(1):1–6

51. Kim DH, Szanyi J, Kwak JH, Szailer T, Hanson J, Wang CM, Peden CHF (2006) Effect of barium loading on the desulfation of Pt-BaO/Al_2O_3 studied by H_2 TPRX, TEM, sulfur k-edge XANES, and in Situ TR-XRD. J Phys Chem B 110(21):10441–10448

52. Ali SM, Aziz S (1965) Reduction of barites with charcoal. Pak J Sci Res 8(3):136–140

53. Akhmetov TG (1972) Side reactions during the production of barium sulphide melt. Khim Prom-st (Moscow) 48:288–289

54. Adinata D, Daud WMAW, Aroua MK (2007) Preparation and characterization of activated carbon from palm shell by chemical activation with K_2CO_3. Bioresour Technol 98(1):145–149

55. Younas M, Leong LK, Mohamed AR, Sethupathi S (2016) CO_2 adsorption by modified palm shell activated carbon (PSAC) via chemical and physical activation and metal impregnation. Chem Eng Commun 203(11):1455–1463

56. Merck (2023) Sulfuric acid 95–98% EMPROVE® ESSENTIAL Ph Eur,BP,JPE,NF. https://www.merckmillipore.com/MY/en/product/msds/MDA_CHEM-100713?Origin=PDP. Accessed 18 Sep 2023

57. LibreTexts (2023) Infrared: Interpretation, LibreTexts. https://chem.libretexts.org/Bookshelves/Physical_and_Theoretical_Chemistry_Textbook_Maps/Supplemental_Modules_(Physical_and_Theoretical_Chemistry)/Spectroscopy/Vibrational_Spectroscopy/Infrared_Spectroscopy/Infrared%3A_Interpretation. Accessed 6 May 2023

58. Horn AB, Sully KJ (1999) ATR-IR spectroscopic studies of the formation of sulfuric acid and sulfuric acid monohydrate films. Phys Chem 1:3801–3806

59. Merck (2023) IR spectrum table & chart, Merck. https://www.sigmaaldrich.com/MY/en/technical-documents/technical-article/analytical-chemistry/photometry-and-reflectometry/ir-spectrum-table. Accessed 6 May 2023

60. Morsch L, Farmer S, Cunningham K, Sharrett Z (2023) 9.2: Preparation of Alkynes - Elimination Reactions of Dihalides, LibreTexts. https://chem.libretexts.org/Bookshelves/Organic_Chemistry/Organic_Chemistry_(Morsch_et_al.)/09%3A_Alkynes_-_An_Introduction_to_Organic_Synthesis/9.02%3A_Preparation_of_Alkynes_-_Elimination_Reactions_of_Dihalides. Accessed 1 Sep 2023

61. Bader N, Abdelmottaleb O (2017) CO_2 activation of olive bagasse for hydrogen storage. Environ Prog Sustain 36(1):315–324

62. Daud WMAW, Ali WSW (2004) Comparison on pore development of activated carbon produced from palm shell and coconut shell. Bioresour Technol 93(1):63–69

63. Nasri NS, Hamza UD, Ismail SN, Ahmed MM, Mohsin R (2014) Assessment of porous carbons derived from sustainable palm solid waste for carbon dioxide capture. J Clean Prod 71:148–157

64. Rashidi NA, Yusup S (2017) Potential of palm kernel shell as activated carbon precursors through single stage activation technique for carbon dioxide adsorption. J Clean Prod 168:474–486

65. Sumathi S, Bhatia S, Lee KT, Mohamed AR (2009) Optimization of microporous palm shell activated carbon production for flue gas desulphurization: Experimental and statistical studies. Bioresour Technol 100(4):1614–1621

66. Guo J, Luo Y, Lua AC, Chi RA, Chen YL, Bao XT, Xiang SX (2007) Adsorption of hydrogen sulphide (H$_2$S) by activated carbons derived from oil-palm shell. Carbon 45(2):330–336

67. Arami-Niya A, Daud WMAW, Mjalli FS (2010) Using granular activated carbon prepared from oil palm shell by ZnCl$_2$ and physical activation for methane adsorption. J Anal Appl Pyrolysis 89(2):197–203

68. Arami-Niya A, Daud WMAW, Mjalli FS, Abnisa F, Shafeeyan MS (2012) Production of microporous palm shell based activated carbon for methane adsorption: Modeling and optimization using response surface methodology. Chem Eng Res Des 90(6):776–784

69. Meagher MJ, Leone B, Turnbull TL, Ross RD, Zhang ZY, Roeder RK (2013) Dextran-encapsulated barium sulfate nanoparticles prepared for aqueous dispersion as an X-ray contrast agent. J Nanopart Res 15:1–10